future internet

MDPI

Article

Intrusion Detection in the Structure of Signal-Code Design in Cyber-Physical Systems of Swarm Small Aerial Vehicles Group Interaction

Vadim A. Nenashev [1], Renata I. Chembarisova [1], Svetlana S. Dymkova [2,3,*] and Oleg V. Varlamov [2,3]

[1] Department of Design and Technology of Electronic and Laser Devices, Saint-Petersburg State University of Aerospace Instrumentation, 190000 St. Petersburg, Russia; nenashev.va@gmail.com (V.A.N.); renatachembarisova@yandex.ru (R.I.C.)
[2] Scientific Research Department, Moscow Technical University of Communications and Informatics, 111024 Moscow, Russia; vov@mtuci.ru
[3] Institute of Radio and Information Systems (IRIS), 1010 Vienna, Austria
* Correspondence: ds@media-publisher.eu

Abstract

The fault tolerance of a swarm of small aerial vehicles (SAVs) is directly dependent on the reliability of data transmitted over communication channels. One of the key threats is the intentional distortion of signal sequences by an attacker, such as Barker codes or M-sequences, which are used for synchronization and control of the swarm. Such an attack can disable the entire swarm. The aim of this study is to develop a method for detecting such intrusions. The proposed algorithm analyzes mathematical expressions that describe the sidelobes' levels of the autocorrelation function of the code. This approach not only detects unauthorized changes but also accurately identifies the location and magnitude of the distorted element. The conducted experiments confirm the high accuracy of the algorithm. The practical significance of the work lies in the possibility of integrating this method into the security subsystem of group interaction for small aerial vehicles. This creates a mechanism for active anomaly detection in communication channels: when a threat is detected, the swarm can respond promptly by switching to a backup channel, requesting data retransmission, or isolating the compromised channel, which in turn enhances the survivability and fault tolerance of the system's functioning within the group.

Keywords: intrusions detection; cyber-physical systems; swarm of small aerial vehicles (SAVs); Barker codes; M-sequences; autocorrelation function; sidelobes; sequence analysis; anomaly; correlation properties

Academic Editors: Olusola Tolulope Odeyomi and Temitayo Olowu

Received: 9 February 2026
Revised: 25 March 2026
Accepted: 28 March 2026
Published: 1 April 2026

1. Introduction

Currently, the development of methods and technologies for jamming and high-speed data transmission over wireless communication channels between elements of a swarm consisting of small aircraft (SA) at various levels of interaction is relevant [1–4]. This requires channels that allow combining spatially distributed positions into a single information exchange system that provides high reliability in the registration of received echoes [5–9].

Traditional methods of information transfer via communication channels include the following restrictions:

1. dependence on frequency licensing;
2. shortage of free licensed frequencies;
3. susceptibility of communication channels to noise.

To overcome these shortcomings, the development and research of a new data transmission system is becoming a pressing task. Such a system must not only transmit information, but also take into account environmental factors, promptly detect anomalies, and assess their impact on the useful signal within a swarm of interacting SA.

One of the current directions for solving the above-described problem and developing data exchange systems is the use of various code sequences in the preamble of the transmitted message [10–13], which help ensure the reliability of the recorded information.

To implement such an information exchange system, it is proposed to use signals modulated by code sequences, in particular Barker codes, M-sequences, and Gold codes. These codes have special correlation properties that ensure relatively low levels of side lobes (SL) of the autocorrelation function (ACF). This factor makes them in demand for generating probing signals in information transmission systems, as well as in other systems for detecting the isolation of a signal from a noise background [14–17].

However, signals received by SA may be subject to various anomalies leading to distortions of their code structure and, as a consequence, to an increase in the SL of the ACF levels [18–20]. Such distortions may arise both due to natural interference in the communication channel and as a result of targeted destructive influences. In conditions of swarm interaction, where the reliability of synchronization and control directly affects the performance of the overall task, the problem of detecting and localizing such distortions becomes important. Existing methods, such as Hamming codes or classical correlation processing, allow either to detect the fact of an error or to record the presence of a signal. However, they do not provide the ability to analyze in detail the structure of the distortion and determine the location of the changed element.

The aim of this study is to develop an algorithm for detecting distortions in signal-code structures used for synchronization and control in swarm systems of SA, based on the analysis of analytical expressions describing the values of the SL of the ACF levels.

The scientific novelty and contribution of this work are determined by the fact that it proposes an algorithm for determining the location and value of an anomalous value in a sequence. This is achieved through the analysis of analytical expressions that describe the lobe levels of its correlation function. This allows not only for detecting the fact of distortion of the received signal, but also for determining with mathematical precision the location of the damaged element in the code structure, as well as calculating the magnitude of its deviation from the reference value. Unlike known approaches, the developed algorithm maintains its effectiveness for both single and multiple distortions and is successfully applied to various types of code sequences, including Barker codes, M-sequences, and Gold codes. Thus, the proposed approach lays the foundation for the creation of an active signal integrity monitoring subsystem operating in real time and integrated directly into the communication protocols of a swarm of small aerial vehicles, which ultimately increases the overall fault tolerance and survivability of the entire system.

The ***second*** section examines similar approaches existing in the literature and analyzes their advantages and disadvantages.

The ***third*** section of the study analyzes traditional binary codes used to modulate received signals under conditions where anomalies distort the structure of code sequences. Their correlation characteristics are examined, and an algorithm is developed to determine the presence, quantity, and magnitude of distortions, as well as the location of anomalies in the code structure, using analytical expression analysis. This analysis uses expressions describing the lobe levels of the periodic ACF (PACF), the aperiodic ACF (AACF), and the

cross-correlation function (CCF) between the received sequence and the code stored in the receiver's memory.

The ***fourth*** section presents the results of computer experiments to detect anomalies in the code structure recorded in the preamble. An algorithm for determining the presence of an anomaly, its value and location in the code sequence, and its impact on the lobe levels of the ACF is tested.

The ***fifth*** section discusses the obtained results and formulates further technical recommendations for their development and implementation in communication systems that integrate SA into a swarm. It also identifies areas for their further application in other areas where interaction between individual swarm elements is required through communication between them to expand their functionality within the framework of developing new hybrid group systems.

The ***sixth*** section summarizes the results of the study and emphasizes the scientific and technical novelty of the results obtained in this work.

2. Related Works

In recent years, significant progress has been made in the development of methods for ensuring the integrity and reliability of signal-code structures used in telecommunications and radar. Particular attention is paid to methods for detecting and correcting distortions arising both from channel noise and from targeted destructive influences. This chapter examines existing approaches, their advantages, and limitations in the context of problems similar to the search for anomalies in the structure of code sequences.

Among the well-known methods of error detection and correction are Hamming codes, proposed by Richard Hamming in 1950. They became the first class of linear block codes capable of not only detecting but also correcting single errors in data blocks. The classic Hamming (7,4) code adds three check bits to four data bits, which makes it possible to correct any single error or detect double errors. The code's operating mechanism is based on parity checking over several overlapping groups of bits, which ultimately forms an error syndrome indicating the specific position of the corrupted bit. Despite their effectiveness for single errors and simplicity of hardware implementation, Hamming codes have limited applicability for detecting complex, multiple corruptions in sequences [21].

Correlation methods are a classic tool for detecting known signals in a noisy environment. In particular, matched filters and CCF computation are widely used for synchronization and detection of signals such as Barker codes [22,23].

The key drawback of these methods in the context of the problem being solved is that they provide only an integral assessment—the presence or absence of a correlation peak. They allow one to detect the fact of signal reception, even if it is highly noisy, but do not provide tools for a detailed analysis of the distortions in its internal structure. If the code sequence has been modified, these methods will record a deterioration in the signal-to-noise ratio and, possibly, a synchronization failure, but will not indicate which specific code element is distorted or the magnitude of this distortion.

Methods for processing M-sequences are known, aimed at compensating for the SL of the ACF to improve the detection of weak signals. However, here too the goal is to suppress the destructive influence on the signal structure, rather than to analyze this structure to identify defects [24].

An analysis of existing methods allows us to identify the key advantages of the developed algorithm, which determine its novelty. Hamming codes merely state the presence of an error and indicate its position. Classical correlation processing, in turn, records only the fact of signal detection. In contrast, the proposed algorithm establishes a direct analytical relationship between the values of the code sequence elements and the

sidelobe levels of its autocorrelation function. This allows not only to detect the fact of distortion but also to mathematically accurately determine its location in the code structure, as well as to calculate the deviation of the distorted element from the reference value. Another important advantage is the algorithm's performance under conditions of multiple distortions. It is also worth noting the invariance of the developed approach to the type of code sequences used: it has been successfully applied to both Barker codes and M-sequences, as well as Gold codes based on them. This demonstrates the universality of the algorithm and opens up prospects for its extension to other classes of codes with good correlation properties, such as Kasami codes, which is one of the areas of further research.

3. Detection of Anomalous Values in the Structure of Code Sequences

A pressing challenge is improving methods and technologies aimed at ensuring high-speed, interference-resistant data transmission in wireless communication channels to facilitate interactions among groups of SA. A key element in creating swarm aviation systems is the integration of distributed transceivers of SA communication equipment into a single system that guarantees reliable and uninterrupted data exchange [25–31].

For reliable transmission of information, a specialized communication protocol is required that uses a method for interpreting received data and dividing the information into frames [32–35]. Each frame contains useful information and a preamble for synchronizing and processing the transmitted data. The frame structure includes a preamble, which is necessary for synchronization and signal identification upon receipt. The preamble must have certain correlation characteristics to ensure reliable detection and minimize the impact of anomalies in its structure.

The key problem, however, remains the susceptibility of the signals received by the receiver to distortions, which lead to a deterioration in the correlation properties, which entails a change in the structure of the signal preamble. This, in turn, has a destructive effect on introducing distortions into the values of the SL of the ACF, which ultimately negatively affects the reliability of the reception of signals transmitted within the swarm [36–41].

When selecting a sequence for preamble modulation, preference is often given to the one with the lowest level of SL of the normalized ACF (NACF). For example, for Barker codes, this level in modulus is equal to 1/N, where N is the code length. These codes are used in the construction of various devices and detection systems, for example, in swarm systems for airborne sensing of the earth's surface [42]. Barker sequences have an advantage in the value of SL of the NACF among all sequences of the same length, which is why these codes are quite in demand in wireless communication systems [43]. Among the code structures used to generate modulated signals, M-sequences are also often used. For any M-sequence of length N, the PACF has a constant BL level equal to $-1/N$.

In this paper, we formulate and solve the problem of developing an algorithm based on the analysis of analytical expressions describing the levels of the ACF lobes, with the aim of detecting anomalies in code sequences. Table 1 shows an example of calculating analytical expressions describing the main and SL of the correlation function using the example of the ACF of the Barker-5 code, where m is the number of the ACF lobe, the number of the main lobe of the ACF is 0.

Figure 1 shows the general algorithm for preprocessing the data required for further operation of the algorithm for searching for anomalies in the structure of signal-code constructions. According to this algorithm, summary tables are constructed, filled with analytical expressions describing the lobes of the correlation functions for all possible combinations of code distortions. First, a table is constructed for the SL of the PACF. If there are no matching columns in this table, then further analysis of the correlation functions of the sequence is not required. If matches are found, then tables are constructed

for the lobes of the AACF, as well as the CCF, with the reference sequence. This way, unique analytical expressions are obtained corresponding to each combination of sequence distortions. Thanks to this, it is possible to determine with high accuracy both the presence of an anomaly and its location in the sequence.

Table 1. Calculation of the lobes of the AACF using the Barker-5 code as an example.

m	**−4**	**−3**	**−2**	**−1**	**0**	**1**	**2**	**3**	**4**
	1	1	1	−1	1				
1	1	1	1	−1	1				
−1		−1	−1	−1	1	−1			
1			1	1	1	−1	1		
1				1	1	1	−1	1	
1					1	1	1	−1	1
	1	0	1	0	5	0	1	0	1

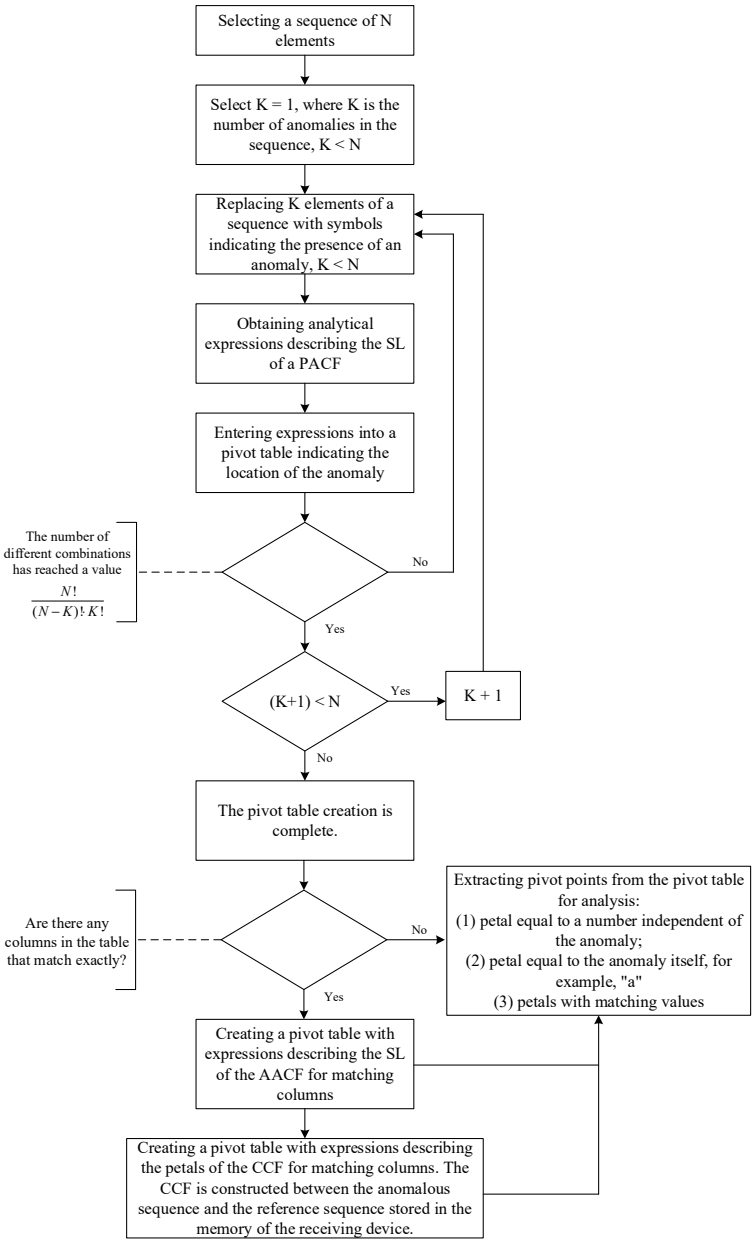

Figure 1. Data preprocessing algorithm.

Figure 2 shows the algorithm for processing the distorted signal-code structure received by the receiver. A correlation function is constructed from the sequence received by the receiver. The lobes of this function are compared at reference points with pre-processed tables of analytical expressions for the lobes of the correlation functions. Based on the comparison results, the location and value of the anomaly are found.

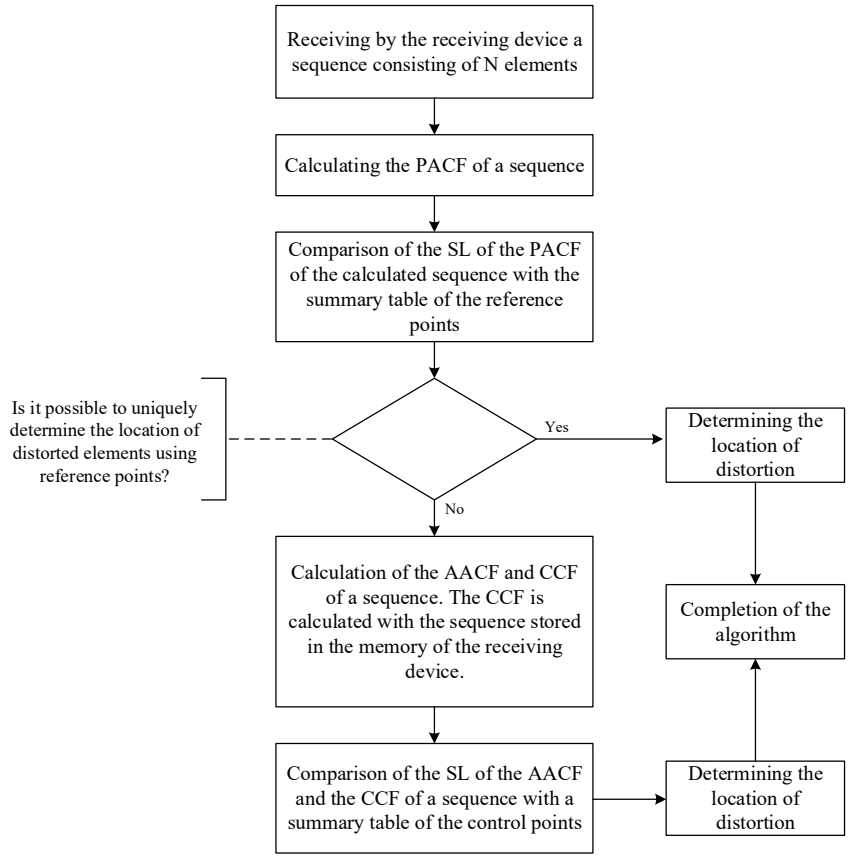

Figure 2. Algorithm for analyzing a distorted sequence.

Figures 3–5 show the process of detecting an anomaly using the example of Barker-5 code analysis, which includes the following steps.

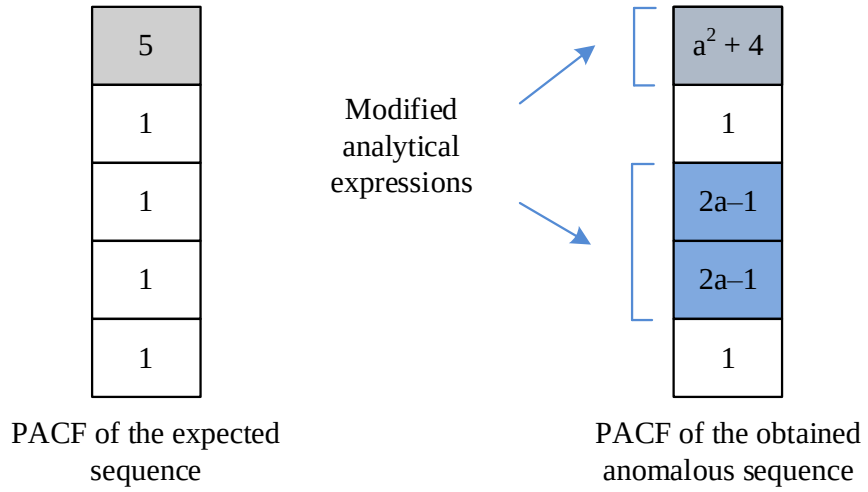

Figure 3. The influence of anomalies on the main and SL of the PACF.

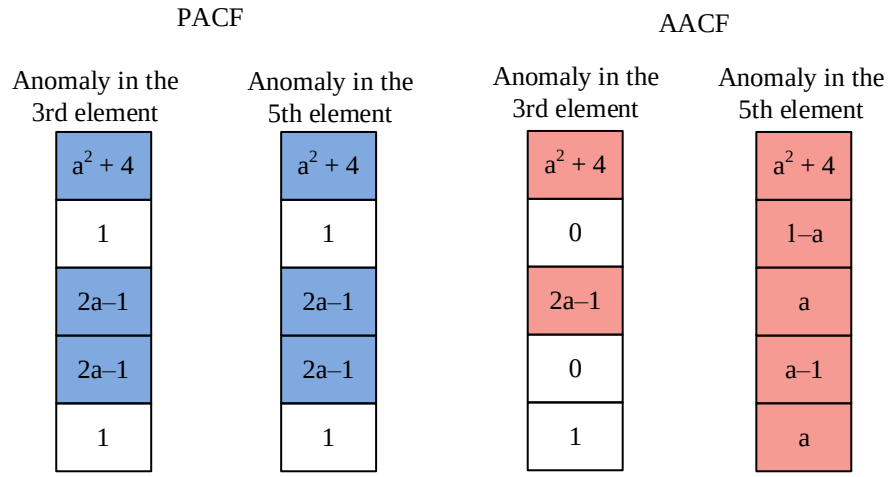

Figure 4. The influence of anomalies on the main and SL of the PACF and AACF.

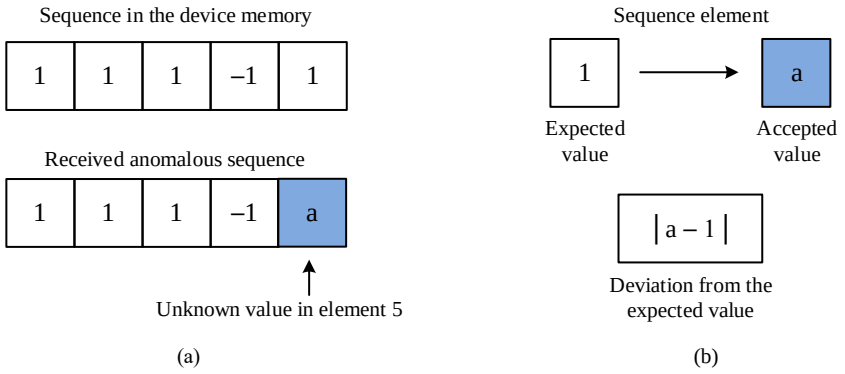

Figure 5. Place and significance of the anomaly in the sequence. (**a**) determination of distortion in the fifth element of the sequence; (**b**) example of deviation from the expected value.

1. Receiving a distorted sequence with an anomaly by the receiver and calculating its PACF. Figure 3 shows an example of analytical expressions describing the main and SL of the PACF in the expected and distorted code sequence using the example of the Barker-5 code. Parameter "a" is the anomalous value. The main lobe is highlighted in dark color.
2. If it is impossible to accurately determine the location of the anomaly distortion from the obtained results of the analytical expressions of the PACF (see Figure 3), then it is necessary to further consider the expressions describing the lobes of the AACF or CCF with the sequence stored in the memory of the receiving device. Figure 4 shows a comparison of the PACF and the AACF of the Barker-5 code with an anomaly in the third or fifth elements of the code structure. Here, the PACF of the two distorted Barker-5 codes completely coincide, but the AACF does not; therefore, the location of the anomaly can be accurately determined using the AACF.
3. Finding the element number where the distortion occurred is based on determining the lobe levels of the correlation function of the preamble modulating sequence. Since the analytical expressions describing the lobes of the PACF do not provide a reliable answer to the location of the distortion, the lobes of the AACF are considered. Figure 4 shows that, while the PACF completely coincides, the sidelobes of the AACF do not completely coincide. When a distortion occurs in the third element, only the main and second side lobes of the AACF are altered, while when a distortion occurs in the fifth element, all lobes of the AACF are altered. Thus, the distortion in the fifth element of the sequence was determined (Figure 5a). After this, the distortion value and the

deviation from the original value are determined. Figure 5b shows an example of a deviation from the expected value.

Thus, Figures 3–5 show the parameters that change in the presence of an anomaly in the code sequence. These figures demonstrate the main stages of the algorithm, including finding the element with the distortion, calculating the magnitude of this distortion, and determining the location of the anomaly's influence on the correlation function.

Since the receiving device that received the signal knows the expected sequence in the preamble, it is possible to calculate the analytical expressions for the PACF, AACF, and CCF of the sequence with anomalies in each position. Table 2 presents the analytical expressions for the main and side lobes of the PACF of the Barker-5 code with anomalies in 1, 2, 3, 4, or 5 elements. For greater clarity, completely matching columns are highlighted in the same colors.

Table 2. Calculation of the main and side lobes of the PACF for the Barker-5 code with one anomaly.

	Location of the Anomaly (Position)					
m	**0**	**1**	**2**	**3**	**4**	**5**
0	5	$a^2 + 4$	$a^2 + 4$	$a^2 + 4$	$a^2 + 4$	$a^2 + 4$
1	1	$2a - 1$	$2a - 1$	1	$2a + 3$	1
2	1	1	1	$2a - 1$	$2a + 3$	$2a - 1$
3	1	1	1	$2a - 1$	$2a + 3$	$2a - 1$
4	1	$2a - 1$	$2a - 1$	1	$2a + 3$	1

Since the table contains completely matching columns, it is impossible to accurately determine the location of the anomaly (in position 2 or 3, or in position 3 or 5) from Table 2. It is worth considering the analytical expressions describing the AACF or CCF with the sequence stored in the device memory. Table 3 presents the analytical expressions describing the lobes of the AACF of the Barker-5 code.

Table 3. Calculation of the main and side lobes of the AACF for the Barker-5 code with one anomaly.

	Location of the Anomaly (Position)					
m	**0**	**1**	**2**	**3**	**4**	**5**
0	5	$a^2 + 4$	$a^2 + 4$	$a^2 + 4$	$a^2 + 4$	$a^2 + 4$
1	0	$a - 1$	$2a - 2$	0	$2a + 2$	$1 - a$
2	1	a	$2 - a$	$2a - 1$	$a + 2$	a
3	0	$1 - a$	$a - 1$	0	$a + 1$	$a - 1$
4	1	a	1	1	1	a

Since there are no completely matching values in Table 3, the location of the anomaly can be determined with high accuracy. Similarly, this can be determined using analytical expressions describing the lobes of the CCF between the anomalous sequence and the one stored in the device's memory (Table 4).

Since there are also no completely matching values in Table 4, it is possible to unambiguously determine the location of the anomaly in the accepted sequence and its deviation from the reference value.

Since it is not always the case that only one element of the sequence contained in the preamble of a frame arriving at the receiver is distorted, it is necessary to also consider the case of a larger number of distorted elements. Thus, as an example, the case of the simultaneous presence of two anomalies in the structure of the code sequence will be considered. Table 5 shows an example of analytical expressions describing the lobes of the

ACF of the Barker-5 code with two anomalies. Parameters "a" and "b" are the distortions. For greater clarity, completely matching columns are highlighted in the same colors.

Table 4. Calculation of the lobes of the CCF between the received anomalous (with one anomaly) and the Barker-5 codes stored in the device memory.

	Location of the Anomaly (Position)					
m	**0**	**1**	**2**	**3**	**4**	**5**
−4	1	a	1	1	1	1
−3	0	1 − a	a − 1	0	0	0
−2	1	a	2 − a	a	1	1
−1	0	a − 1	a − 1	1 − a	a + 1	0
0	5	a + 4	a + 4	a + 4	4 − a	a + 4
1	0	0	a − 1	a − 1	a + 1	1 − a
2	1	1	1	a	a + 2	a
3	0	0	0	0	a + 1	a − 1
4	1	1	1	1	1	a

Table 5. Calculation of the main and side lobes of the PACF for the Barker-5 code with two anomalies.

	Location of the Anomaly (Position)									
m	**1, 2**	**1, 3**	**1, 4**	**1, 5**	**2, 3**	**2, 4**	**2, 5**	**3, 4**	**3, 5**	**4, 5**
−4	a + b + ab − 2	2a − 1	2a + 2b + 1	a − b + ab	a − b + ab	2a + 2b + 1	2a − 1	a + b + ab + 2	1	a + b + ab + 2
−3	1	b − a + ab	a + b + ab + 2	2b − 1	2b − 1	a + b + ab + 2	b − a + ab	2a + 2b + 1	a + b + ab − 2	2a + 2b + 1
−2	1	b − a + ab	a + b + ab + 2	2b − 1	2b − 1	a + b + ab + 2	b − a + ab	2a + 2b + 1	a + b + ab − 2	2a + 2b + 1
−1	a + b + ab − 2	2a − 1	2a + 2b + 1	a − b + ab	a − b + ab	2a + 2b + 1	2a − 1	a + b + ab + 2	1	a + b + ab + 2
0	$a^2 + b^2 + 3$	$a^2 + b^2 + 3$	$a^2 + b^2 + 3$	$a^2 + b^2 + 3$	$a^2 + b^2 + 3$	$a^2 + b^2 + 3$	$a^2 + b^2 + 3$	$a^2 + b^2 + 3$	$a^2 + b^2 + 3$	$a^2 + b^2 + 3$
1	a + b + ab − 2	2a − 1	2a + 2b + 1	a − b + ab	a − b + ab	2a + 2b + 1	2a − 1	a + b + ab + 2	1	a + b + ab + 2
2	1	b − a + ab	a + b + ab + 2	2b − 1	2b − 1	a + b + ab + 2	b − a + ab	2a + 2b + 1	a + b + ab − 2	2a + 2b + 1
3	1	b − a + ab	a + b + ab + 2	2b − 1	2b − 1	a + b + ab + 2	b − a + ab	2a + 2b + 1	a + b + ab − 2	2a + 2b + 1
4	a + b + ab − 2	2a − 1	2a + 2b + 1	a − b + ab	a − b + ab	2a + 2b + 1	2a − 1	a + b + ab + 2	1	a + b + ab + 2

Since the analytical expressions presented in Table 5 do not allow us to understand the exact location of the anomalies. For example, with distortion in positions 1 and 3 and distortion in positions 2 and 5, the lobes are distorted equally. It is necessary to additionally consider the AACF or the CCF with the Barker-5 code stored in the receiver's memory. Table 6 examines the CCF.

As can be seen from Table 6, there are no completely identical changes in the analytical expressions describing the CCF of the Barker-5 code. Therefore, it is advisable to simultaneously consider changes in both the periodic autocorrelation function and the cross-correlation function to accurately determine the location and magnitude of the anomaly.

Next, as an example, similar to the Barker-5 code considered earlier, we will consider two M-sequences of length N = 7, generated by two different generator polynomials presented in Table 7 [44–46].

Table 6. Calculation of the main and side lobes of the CCF for the Barker-5 code with two anomalies.

	Location of the Anomaly (Position)									
m	**1, 2**	**1, 3**	**1, 4**	**1, 5**	**2, 3**	**2, 4**	**2, 5**	**3, 4**	**3, 5**	**4, 5**
−4	a	a	a	a	1	1	1	1	1	1
−3	b − a	1 − a	1 − a	1 − a	a − 1	a − 1	a − 1	0	0	0
−2	a − b + 1	a + b − 1	a	a	b − a + 1	2 − a	2 − a	a	a	1
−1	a + b − 2	a − b	a + b	a − 1	a − b	a + b	a − 1	b − a + 2	1 − a	a + 1
0	a + b + 3	a + b + 3	a − b + 3	a + b + 3	a + b + 3	a − b + 3	a + b + 3	a − b + 3	a + b + 3	b − a + 3
1	b − 1	b − 1	b + 1	1 − b	a + b − 2	a + b	a − b	a + b	a − b	a − b + 2
2	1	b	b + 2	b	b	b + 2	b	a + b + 1	a + b − 1	a + b + 1
3	0	0	b + 1	b − 1	0	b + 1	b − 1	b + 1	b − 1	a + b
4	1	1	1	b	1	1	b	1	b	b

Table 7. M-sequences and their generating polynomials.

№	Generating Polynomial	M-Sequence
1	$x^3 + x^2 + 1$	−1 −1 1 1 1 −1 1
2	$x^3 + x + 1$	1 1 −1 −1 1 −1 1

Further in Table 8 for the M-sequence from Table 7 with number 1, analytical expressions are shown that describe the main and side lobes of the PERIODIC PACF of M-sequences when introducing one anomaly in 1, 2, 3, 4, 5, 6 or 7 elements into the sequence structure.

Table 8. Calculation of the main and side lobes of the PACF for an M-sequence of length N = 7 with a generating polynomial $x^3 + x^2 + 1$.

	Location of the Anomaly (Position)							
m	**0**	**1**	**2**	**3**	**4**	**5**	**6**	**7**
0	7	$a^2 + 6$	$a^2 + 6$	$a^2 + 6$	$a^2 + 6$	$a^2 + 6$	$a^2 + 6$	$a^2 + 6$
1	−1	−1	−1	−1	2a − 3	−1	2a + 1	1 − 2a
2	−1	−1	2a + 1	−1	1 − 2a	2a − 3	−1	−1
3	−1	2a + 1	−1	−1	−1	1 − 2a	−1	2a − 3
4	−1	2a + 1	−1	−1	−1	1 − 2a	−1	2a − 3
5	−1	−1	2a + 1	−1	1 − 2a	2a − 3	−1	−1
6	−1	−1	−1	−1	2a − 3	−1	2a + 1	1 − 2a

As can be seen from Table 8, there are no completely matching columns when one anomaly appears; therefore, there is no need to consider the AACF or the CCF. Table 9 similarly presents the analytical expressions for M-sequence No. 2 from Table 7.

Table 9. Calculation of the main and side lobes of the PACF for an M-sequence of length N = 7 with a generating polynomial $x^3 + x + 1$.

	Location of the Anomaly (Position)							
m	**0**	**1**	**2**	**3**	**4**	**5**	**6**	**7**
0	7	$a^2 + 6$	$a^2 + 6$	$a^2 + 6$	$a^2 + 6$	$a^2 + 6$	$a^2 + 6$	$a^2 + 6$
1	−1	2a − 3	−1	−1	−1	1 − 2a	2a + 1	−1
2	−1	1 − 2a	−1	2a + 1	−1	−1	−1	2a − 3
3	−1	−1	−1	−1	2a + 1	2a − 3	−1	1 − 2a
4	−1	−1	−1	−1	2a + 1	2a − 3	−1	1 − 2a
5	−1	1 − 2a	−1	2a + 1	−1	−1	−1	2a − 3
6	−1	2a − 3	−1	−1	−1	1 − 2a	2a + 1	−1

Comparing the values from Tables 8 and 9, it is clear that they have matching columns. To accurately determine the location and magnitude of the anomalous value, it is necessary to know which specific M-sequence the receiving device should receive.

For the Gold code, constructed based on the M-sequences from Table 7, it is also necessary to construct summary tables for analysis. Thus, Table 10 shows the change in the analytical expressions describing the SL of the PACF of the Gold code with one anomaly, constructed from M-sequence №1 and M-sequence №2, cyclically shifted by 6 positions. The Gold code looks as follows: [1 –1 1 –1 1 1 –1].

Table 10. Calculation of the main and side lobes of the PACF for the Gold code of length N = 7.

	Location of the Anomaly (Position)							
m	**0**	**1**	**2**	**3**	**4**	**5**	**6**	**7**
0	7	$a^2 + 6$	$a^2 + 6$	$a^2 + 6$	$a^2 + 6$	$a^2 + 6$	$a^2 + 6$	$a^2 + 6$
1	-5	$-2a - 3$	$2a - 3$	$-2a - 3$	$2a - 3$	-5	-5	$2a - 3$
2	3	$2a + 1$	$1 - 2a$	$2a + 1$	3	3	3	3
3	-1	-1	$2a + 1$	-1	-1	-1	-1	-1
4	-1	-1	$2a + 1$	-1	-1	-1	-1	-1
5	3	$2a + 1$	$1 - 2a$	$2a + 1$	3	3	3	3
6	-5	$-2a - 3$	$2a - 3$	$-2a - 3$	$2a - 3$	-5	-5	$2a - 3$

As can be seen in Table 10, there are completely matching columns, so another pivot table must be constructed to accurately determine the location and value of the anomaly. Table 11 shows a pivot table with analytical expressions describing the SL of the AACF for the Gold code.

Table 11. Calculation of the main and side lobes of the AACF for the Gold code of length N = 7.

	Location of the Anomaly (Position)							
m	**0**	**1**	**2**	**3**	**4**	**5**	**6**	**7**
0	7	$a^2 + 6$	$a^2 + 6$	$a^2 + 6$	$a^2 + 6$	$a^2 + 6$	$a^2 + 6$	$a^2 + 6$
1	-4	$-a - 3$	$2a - 2$	$-2a - 2$	$2a - 2$	-4	-4	$a - 3$
2	1	a	$-a$	$2a - 1$	1	1	$2 - a$	$a + 2$
3	0	$1 - a$	$a + 1$	$a - 1$	0	$1 - a$	$a - 1$	$-a - 1$
4	-1	$a - 2$	a	$-a$	-1	$a - 2$	$-a$	a
5	2	$a + 1$	$1 - a$	2	2	2	$a + 1$	$1 - a$
6	-1	$-a$	-1	-1	-1	-1	-1	a

As can be seen from Table 11, there are no completely identical changes in the analytical expressions describing the AACF of the Gold code. Therefore, it is advisable to simultaneously consider changes in both the PACF and the AACF to accurately determine the location and magnitude of the anomaly.

Analyzing Tables 2–11, we can conclude that to determine anomalies in a sequence received by a receiver, it may be necessary to consider not only the analytical expressions describing the lobes of the PACF, but also the expressions determining the lobe levels of the AACF or CCF. For longer sequences, tables are constructed in a similar manner. This algorithm is applicable to sequences of any length.

4. Computer Experiments for Anomaly Detection in Sequence Structure

To better understand the anomaly detection algorithm discussed in Section 3, several numerical examples of their search should be examined. For this purpose, experiments on

searching for distortions in the structure of the Barker-5 code (one and two distortions), the M-sequence (one distortion), and the Gold code (one distortion) are presented below.

4.1. Experiment with One Distortion in the Structure of the Barker Code

Let the receiving device receive a synchronizing signal whose preamble contains a Barker-5 code. The expected PACF of this code is shown in Figure 6a. The receiver receives a signal with a distorted preamble, the PACF of which is shown in Figure 6b. The vertical axis shows the values of the lobes of the PACF, and the horizontal axis shows the lobe number. It is necessary to determine where exactly the anomalous value is located in the sequence structure.

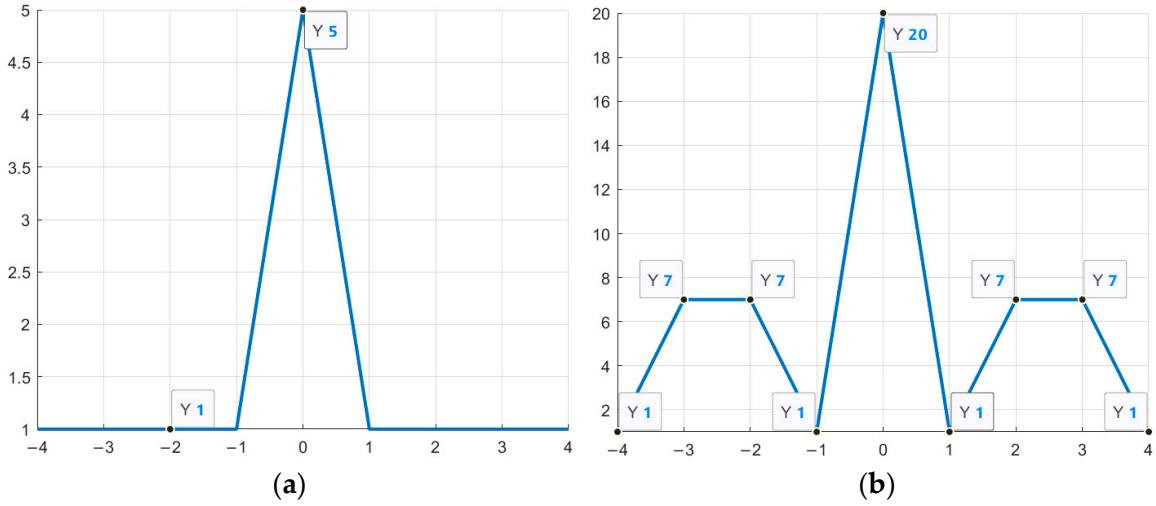

Figure 6. PACF of the Barker-5 code: (**a**) Reference; (**b**) Distorted by one anomaly.

As can be seen from Figure 6, the main and several side lobes (±2 and ±3) of the PACF of the received distorted sequence are changed. Since these lobes are distorted both with an anomaly in position 3 and with an anomaly in position 5, it is impossible to determine the magnitude of the distortion precisely. It is also necessary to additionally examine the graphs of the AACF, which are presented in Figure 7 (Figure 7a shows the reference AACF, Figure 7b shows the distorted one).

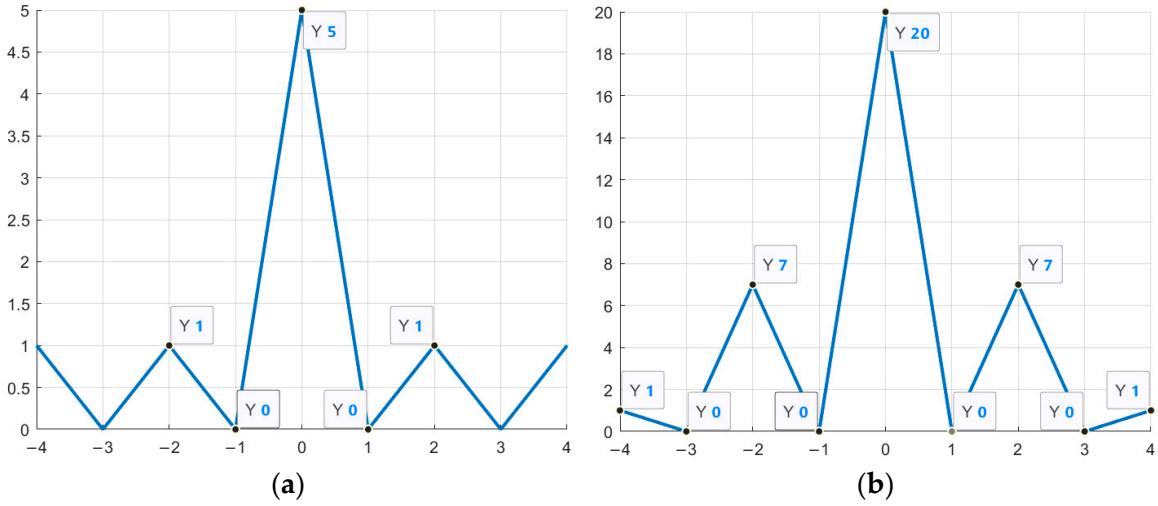

Figure 7. AACF of the Barker-5 code: (**a**) Reference; (**b**) Distorted by one anomaly.

As can be seen from Figure 7a,b, in the AACF of the distorted sequence, only the main lobe and ±2 side lobe are changed. From this, we can conclude that the anomalous value of the Barker-5 reference sequence (Figure 8a) is located precisely in the third element of the code (Figure 8b).

(**a**) (**b**)

Figure 8. Accepted Barker code-5: (**a**) Reference; (**b**) Distorted by one anomaly.

So, after the location of the anomaly has been determined, the magnitude of the distortion must also be determined. The second side lobe is described by the expression (2a − 1) and is equal to 7; therefore, the desired anomaly value "a" is equal to 4. Thus, in order to identify the anomaly in the Barker-5 code, it was necessary to consider analytical expressions describing not only the PACF, but also the AACF.

4.2. Experiment with One Distortion in the Structure of the M-Sequence

As a second example, we can consider a distortion in one of the M-sequences considered earlier. Thus, Figure 9 shows the PACF of the M-sequence with the generator polynomial $x^3 + x^2 + 1$ without the anomaly (Figure 9a) and with it (Figure 9b).

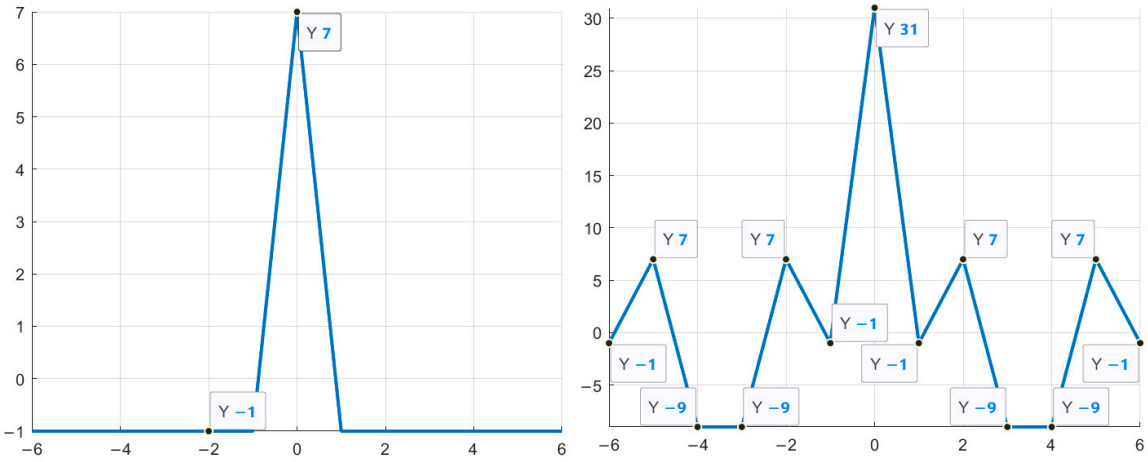

(**a**) (**b**)

Figure 9. PACF of an M-sequence with a generating polynomial $x^3 + x^2 + 1$: (**a**) Reference; (**b**) Distorted.

Since in Table 6, where all the analytical expressions describing the lobes of the PACF for the M-sequence under consideration are described, there are no completely coinciding columns, which means that the obtained PACF is sufficient to determine the location of the anomaly in the code. Thus, in Figure 9, it is evident that ±2, ±3, ±4, and ±5 side lobes and the main one are distorted. Such a distortion corresponds to an anomaly in the fifth element of the M-sequence (in Figure 10a—the reference sequence, in Figure 10b—the distorted).

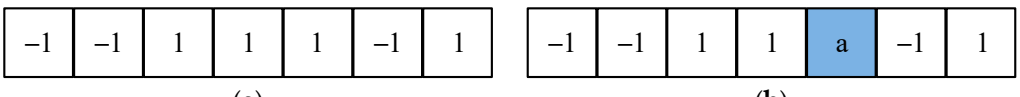

(**a**) (**b**)

Figure 10. The accepted M-sequence: (**a**) Reference; (**b**) Distorted.

The location of the anomaly has been determined, so its magnitude can be determined using any of the expressions describing the distorted SL. The fourth side lobe is described by the expression (1 − 2a) and is equal to –9; therefore, the sought value of the anomaly "a" is equal to 5. Thus, in order to identify one anomaly in the structure of the M-sequence, it was necessary to consider analytical expressions describing only the PACF.

4.3. Experiment with Two Distortions in the Structure of the Barker-5 Code

As a final example, we will consider a Barker-5 code with two anomalies in the code structure. Figure 11 shows the PACF of the reference (Figure 11a) and corrupted (Figure 11b) Barker-5 codes.

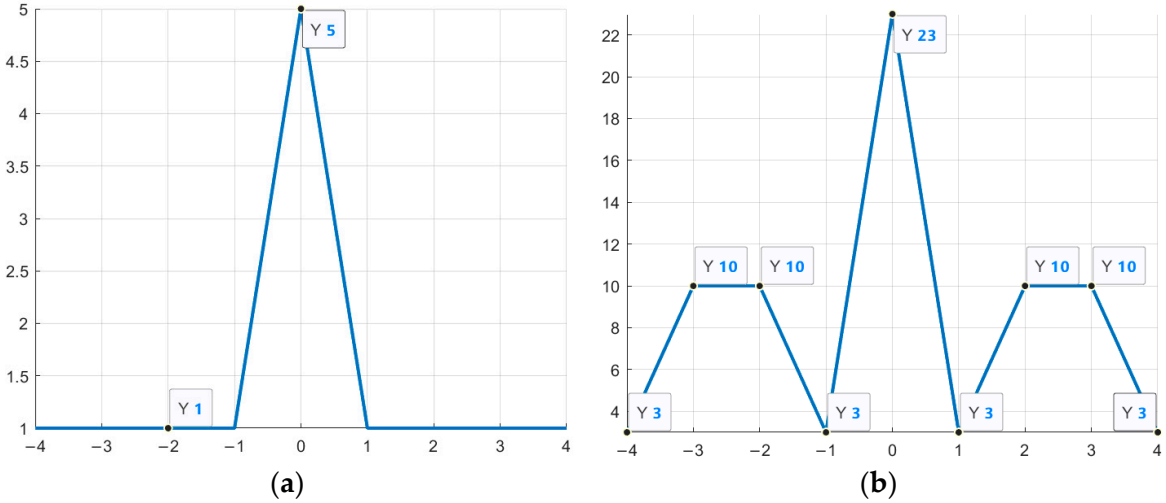

Figure 11. PACF of the Barker-5 code: (**a**) Reference; (**b**) Distorted by two anomalies.

As can be seen from Figure 11, absolutely all lobes of the PACF are distorted, which does not allow us to accurately determine the location of the anomaly, since all lobes are distorted in 8 out of 10 variants of two distortions (only 1, 2 or 3, 5 distortion variants are excluded). Figure 12 shows the change in the CCF. The CCF of the reference code with the code stored in the memory of the receiving device coincides with the AACF of the reference code.

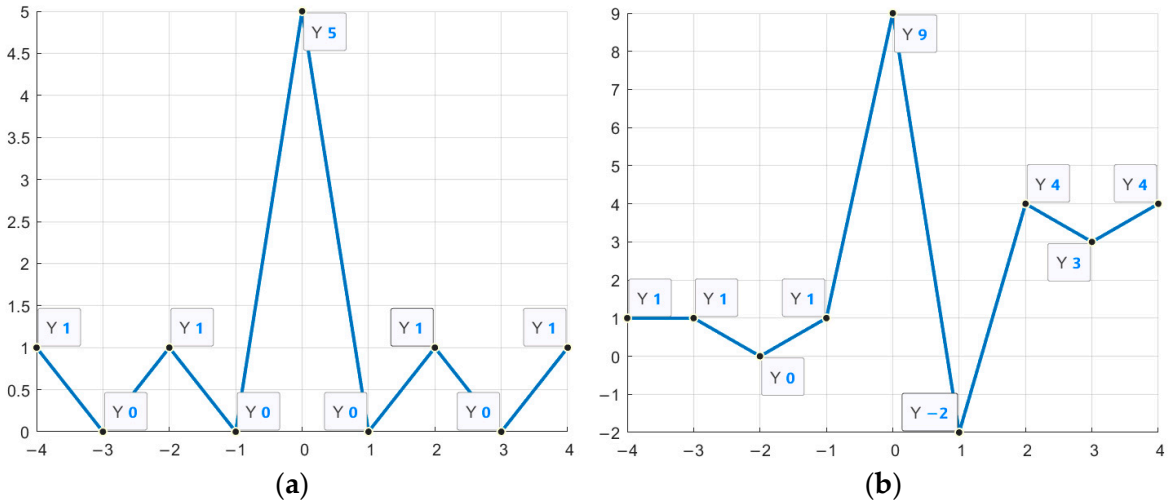

Figure 12. CCF of the Barker-5 code: (**a**) Reference; (**b**) Distorted by two anomalies.

In this case, analyzing the obtained result is more difficult; it is worth starting the check with the side lobe with the number m = −4. If the first element of the Barker-5 code

is distorted, then this lobe has a value equal to the distorted element. Here, this lobe is equal to 1; therefore, there is no distortion in the first element of the sequence received by the receiver.

Next, it is worth paying attention to the last side lobe with the number m = 4. This lobe changes in only 3 out of 10 cases: with distortion in the 2nd and 5th code positions, 3rd and 5th positions, and 4th and 5th positions. The variant of distortion in the 3rd and 5th positions of the Barker-5 code was excluded at the stage of consideration of the PACF, so only two possible sequence distortions remain.

Since the lobe with number m = 5 has a value equal to the distorted element and is equal to 4, it is sufficient to check the value of the other lobes by substituting this value into the analytical expressions describing them. Then, after substituting the value of one of the anomalies, the analytical expressions for the two remaining possible distortions will be shown in Table 12.

Table 12. Calculation of the main and side lobes of the CCF for the Barker-5 code with two anomalies at 2.5 positions and at 4.5 positions.

m	−4	−3	−2	−1	0	1	2	3	4
Anomaly in positions 2, 5	1	a − 1	2 − a	a − 1	a + 7	a − 4	4	3	4
Anomaly in positions 4, 5	1	0	1	a + 1	7 − a	a − 2	a + 5	a + 4	4

Thus, based on the results of Table 12, the anomalies are located in positions 2 and 5 of the Barker-5 code (Figure 13). The second distortion, located in position 2, is equal to 2.

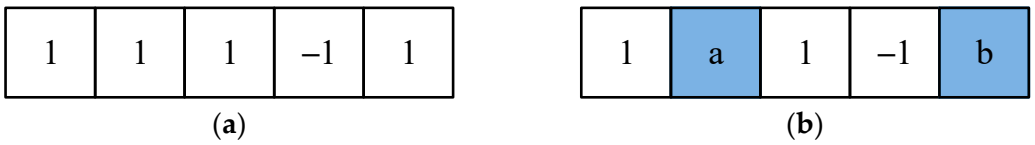

Figure 13. Accepted Barker-5 code: (**a**) Reference; (**b**) Distorted by two anomalies.

So, the location and significance of the anomaly have been determined, which proves the efficiency of the algorithm with M-sequences.

4.4. Experiment with One Distortion in the Structure of the Gold Code

Next, we can consider a Gold code constructed from the two M-sequences described earlier. Let us assume that the receiving device receives a synchronizing signal whose preamble contains a Gold code; the expected PACF of this code is shown in Figure 14a. The receiver receives a signal with a distorted preamble, the PACF of which is shown in Figure 14b.

As can be seen from Figure 14, only the main lobe of the PACF of the received distorted sequence has been changed. Since such a distortion occurs both with a change in 5 and with a change in 6 elements of the sequence, it is impossible to determine the exact location of the anomaly. However, it is possible to determine the magnitude of the distortion, since only the main lobe, which is always described by the expression a2 + 6, is distorted. Since the main lobe of the distorted sequence is 15, the distorted element is 3. It is necessary to examine the graphs of the AACF to find the exact location of the anomaly. The graphs are shown in Figure 15 (Figure 15a shows the reference AACF, Figure 15b shows the distorted one).

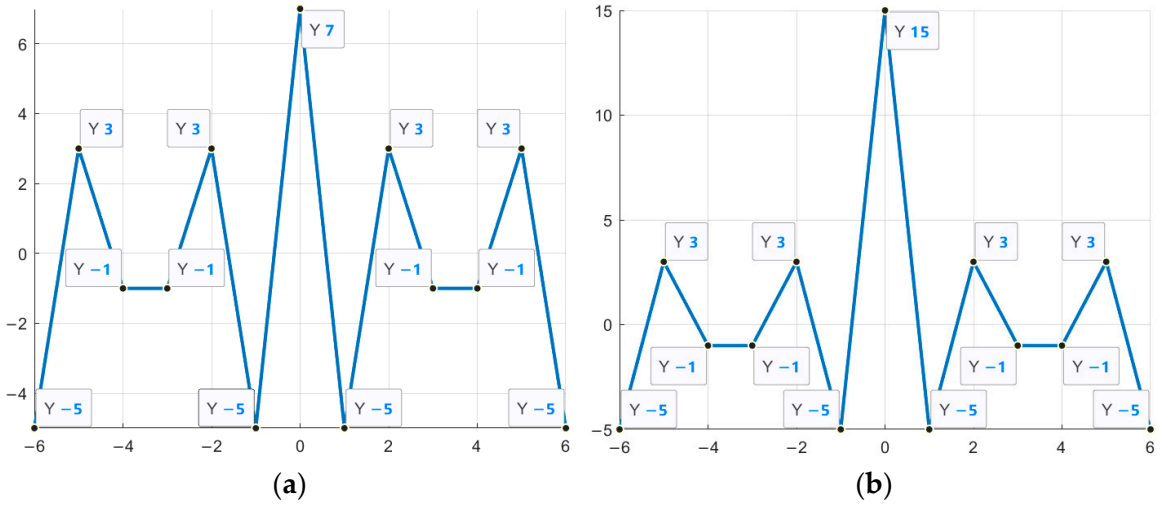

Figure 14. PACF of the Gold code: (**a**) Reference; (**b**) Distorted.

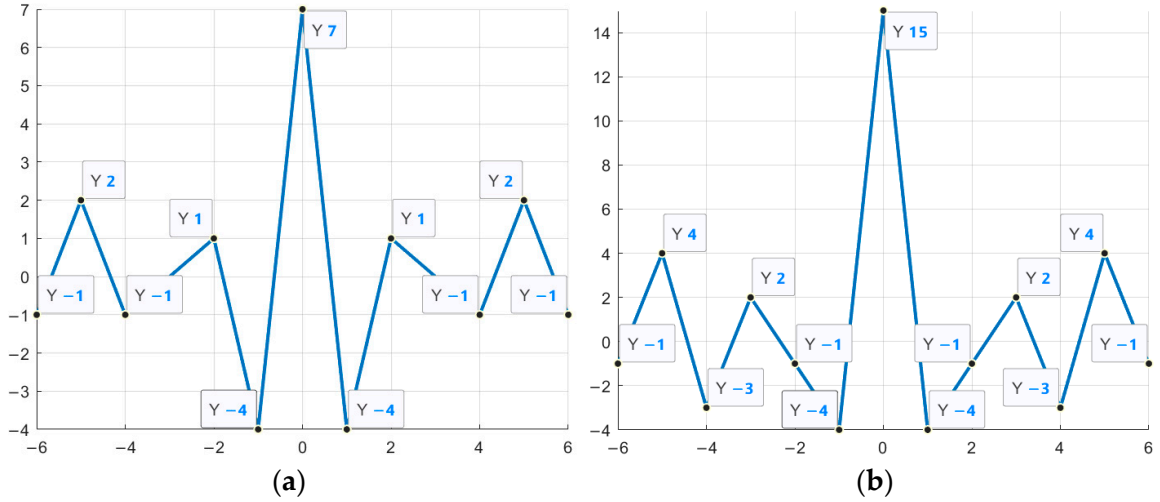

Figure 15. AACF of the Gold code: (**a**) Reference; (**b**) Distorted.

To determine the exact location of the anomaly, it is sufficient to substitute the already found distortion value into the analytical expression describing one of the side lobes of the AACF. For example, the second SL of the AACF is described by expression $2 - a$ when the 6th element of the Gold code is distorted. If the 5th element is distorted, then the second SL of the AACF is equal to 1. As can be seen from Figure 15, the second SL of the AACF is equal to -1; therefore, it is the 6th element that is distorted (Figure 16).

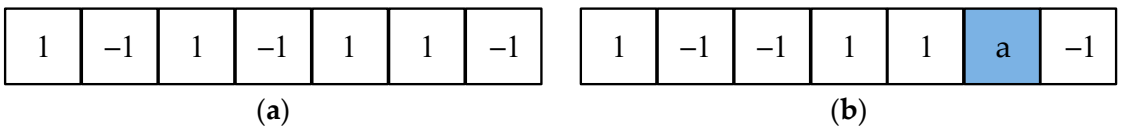

Figure 16. Accepted Gold Code: (**a**) Reference; (**b**) Distorted.

Thus, based on the given examples, the considered values of the PACF lobes are not sufficient; therefore, it becomes necessary to also consider the AACF or CCF with the code stored in the memory of the receiving device.

5. Discussion

The proposed algorithm for detecting anomalies in signal-code structures, based on the analysis of analytical expressions for the levels of the SL of the ACF, has demonstrated high

efficiency when applied to Barker codes, M-sequences, and Gold codes. The experimental results confirm that the developed algorithm is capable of not only detecting the presence of distortion in the code structure of the preamble, but also localizing the position of the modified element with high accuracy and estimating the magnitude of its deviation from the reference value. This is achieved through a combined analysis of the periodic, aperiodic, and cross-correlation functions, which allows one to overcome the ambiguities that arise when using only one type of correlation analysis, especially in cases of multiple distortions.

A key advantage of the approach is its analytical framework, which enables highly accurate anomaly detection. This makes the algorithm particularly promising for resource-constrained real-time systems, such as small aircraft swarm communication systems. The algorithm can be integrated into communication protocols as an additional security loop, continuously monitoring the integrity of synchronization sequences. Upon detecting an anomaly, the swarm communication system can promptly initiate protective measures: switching to a backup communication channel, requesting data retransmission, or isolating the compromised node, thereby increasing the overall survivability and fault tolerance of the data exchange system.

The development of methods and technologies for interference-resistant and high-speed data transmission via wireless communication channels is a key factor for the effective interaction of a group of small aircraft. Implementing multi-position onboard systems requires integrating spatially distributed positions into a single network for reliable information exchange. In this context, the developed algorithm for analyzing signal-code structures plays an important role, as it allows the system not only to detect the presence of distortions but also to assess the potential for destructive impacts, whether natural noise or targeted attacks.

Classic wireless data transmission methods suffer from such shortcomings as the need for frequency licensing and their scarcity, channel noise pollution, and high channel load. The proposed approach to detecting signal preamble distortions minimizes the impact of these factors, ensuring interference-resistant and noise-free information exchange between the communication equipment of small aircraft interacting in a group.

For further development of this area of research, the following is advisable.

1 Expand the scope of the algorithm to other classes of noise-resistant codes widely used in modern communication systems (for example, Kasami codes).
2 Adapt the algorithm to work under conditions of real channel distortions, including the effects of multipath propagation, Doppler frequency shift and clock synchronization instability.

The potential applications of the work's results are not limited to unmanned aircraft. The proposed algorithm may be useful in other areas requiring reliable and secure interactions between distributed system elements. This includes the Industrial Internet of Things (IoT), as well as future-generation mobile networks (5G/6G), where ensuring signal integrity at the physical level is a key challenge. Thus, the research lays the foundation for the creation of new hybrid group systems, whose elements are connected via wireless communication, with expanded functionality and increased resilience to external destructive influences.

6. Conclusions

The paper solves the problem of detecting and analyzing destructive distortions in synchronizing signal-code structures used in group interaction systems, such as swarms of SA.

The main result is the development of a new algorithm that analyzes analytical expressions for the lobes of correlation functions. Based on this analysis, the algorithm not

only detects changes in the signal modulated by the code in the frame preamble, but also accurately localizes the changed elements and estimates the magnitude of the distortion. The proposed anomaly detection approach is effective for various types of sequences, including Barker codes, M-sequences, and Gold codes, and operates under conditions of both single and multiple distortions.

The practical significance of this work lies in the development of an approach for implementing the process of detecting distortions at the physical level of data transmission within a swarm. The algorithm can be integrated into real-time subsystems. This enables a transition from passive information reception to active sequence integrity monitoring, which is a key factor in increasing the reliability of incoming synchronization signals in distributed autonomous systems.

Author Contributions: Conceptualization, R.I.C. and V.A.N.; methodology, R.I.C.; software, V.A.N.; validation, S.S.D., R.I.C. and V.A.N.; formal analysis, S.S.D.; investigation, O.V.V.; resources, R.I.C.; data curation, O.V.V.; writing—original draft preparation, O.V.V.; writing—review and editing, S.S.D.; visualization, V.A.N.; supervision, O.V.V.; project administration, R.I.C.; funding acquisition, S.S.D. All authors have read and agreed to the published version of the manuscript.

Funding: The research of Vadim A. Nenashev and Renata I. Chembarisova was supported by a grant from the Russian Science Foundation (project No. 24-79-10259).

Data Availability Statement: The original contributions presented in this study are included in the article. Further inquiries can be directed to the corresponding author.

Conflicts of Interest: The authors declare no conflicts of interest.

References

1. Deng, C.; Fang, X. Target Allocation and Air–Ground Coordination for UAV Cluster Airspace Security Defense. *Drones* **2025**, *9*, 777. [CrossRef]
2. Zhao, Z.; Chen, S.; Ru, L.; Hu, G.; Wang, W. A Quality Evaluation Method for Drone Swarm Command and Control Networks Based on Complex Network. *Drones* **2025**, *9*, 839. [CrossRef]
3. Li, H.; Li, P.; Liu, J.; Zhang, P. Secure Communication and Dynamic Formation Control of Intelligent Drone Swarms Using Blockchain Technology. *Information* **2025**, *16*, 768. [CrossRef]
4. Ateya, A.A.; Tu, N.D.; Muthanna, A.; Koucheryavy, A.; Kozyrev, D.; Sztrik, J. QL-AODV: Q-Learning-Enhanced Multi-Path Routing Protocol for 6G-Enabled Autonomous Aerial Vehicle Networks. *Future Internet* **2025**, *17*, 473. [CrossRef]
5. Zhang, L.; Tu, G.; Xu, Y.; Zhou, X. A Lightweight CNN-Based Method for Micro-Doppler Feature-Based UAV Detection and Classification. *Electronics* **2025**, *14*, 4831. [CrossRef]
6. Nenashev, V.A.; Shepeta, A.P.; Kryachko, A.F. Fusion Radar and Optical Information in Multi-Position on-Board Location Systems. In Proceedings of the 2020 Wave Electronics and its Application in Information and Telecommunication Systems (WECONF), St. Petersburg, Russia, 1–5 June 2020. [CrossRef]
7. Noda, F.; Tran, G.K. Population Estimation and Scanning System Using LEO Satellites Based on Wireless LAN Signals for Post-Disaster Areas. *Future Internet* **2025**, *17*, 570. [CrossRef]
8. Luo, S. Sensing User Intent: An LLM-Powered Agent for On-the-Fly Personalized Virtual Space Construction from UAV Sensor Data. *Sensors* **2025**, *25*, 7610. [CrossRef]
9. Nenashev, V.A.; Khanykov, I.G. Formation of a complex image of the earth's surface based on clustering of pixels of location images in a multi-position onboard system. *Inform. Autom.* **2021**, *20*, 302–340. [CrossRef]
10. Sun, J.; Jing, G.; Ding, J. Optimization of Dynamic Frame Length for Random Access in Machine-Type Communication Systems. *Electronics* **2025**, *14*, 3414. [CrossRef]
11. Martins, J.; Conceição, F.; Gomes, M.; Silva, V.; Dinis, R. Joint Channel Estimation and Synchronization Techniques for Time-Interleaved Block-Windowed Burst OFDM. *Appl. Sci.* **2021**, *11*, 4403. [CrossRef]
12. Li, L.; Han, Y.; Li, Z.; Li, H.; Lv, J.; Li, Y. Robust Symbol and Frequency Synchronization Method for Burst OFDM Systems in UAV Communication. *Drones* **2024**, *8*, 425. [CrossRef]
13. Crocetti, L.; Pagani, E.; Bertolucci, M.; Fanucci, L. Scalable Hardware-Efficient Architecture for Frame Synchronization in High-Data-Rate Satellite Receivers. *Electronics* **2024**, *13*, 668. [CrossRef]

14. Grigoriev, E.K.; Nenashev, V.A.; Sergeev, A.M.; Nenashev, S.A. Research and analysis of methods forgenerating and processing new code structures for the problems of detection, synchronization and noise-resistant coding. In *Image and Signal Processing for Remote Sensing XXVI*; SPIE: Bellingham, WA, USA, 2020; Volume 11533. [CrossRef]
15. Xiong, F.; Wang, H.; Li, A.; Yu, D.; Wu, G. Compressed sensing-Based Multi-Abnormality Self-Detecting and Faults Location Method For UAV Swarms. *IEICE Trans. Commun.* **2019**, *E102-B*, 1975–1982. [CrossRef]
16. Li, J.; Li, Z.; He, Y.; Li, K.; Chen, H. A Dynamic Compensation Method Based on Pulse Width for Laser Ranging and Distance Determination in Precision-Guided Aircraft. *Micromachines* **2025**, *16*, 1409. [CrossRef]
17. Sysak, D.; Byndas, A.; Karas, T.; Jaromi, G. Lightweight and Compact Pulse Radar for UAV Platforms for Mid-Air Collision Avoidance. *Sensors* **2025**, *25*, 7392. [CrossRef]
18. Batur Dinler, Ö. UAV Cybersecurity with Mamba-KAN-Liquid Hybrid Model: Deep Learning-Based Real-Time Anomaly Detection. *Drones* **2025**, *9*, 806. [CrossRef]
19. Wang, J.; Xiao, Y.; Li, T.; Chen, P.C.L. Position Spoofing Attacks on Unmanned Surface Vehicles. *J. Mar. Sci. Eng.* **2025**, *13*, 2269. [CrossRef]
20. Laktionov, I.; Diachenko, G.; Moroz, D.; Getman, I. A Comprehensive Review of Cybersecurity Threats to Wireless Infocommunications in the Quantum-Age Cryptography. *IoT* **2025**, *6*, 61. [CrossRef]
21. Hamming, R.W. *Coding Theory and Information Theory*; Radio and Communications: Moscow, Russia, 1983.
22. Al-Qawasmi, A.-R.; Al-Lawama, A. Orthogonal frequency division multiplexing based DS-SS Barker code for resistance to AWGN and multipath. In *Photonics Applications in Astronomy, Communications, Industry, and High-Energy Physics Experiments 2010*; SPIE: Bellingham, WA, USA, 2010; Volume 7745. [CrossRef]
23. Li, W.-Y.; Lu, Z.; Li, J.-D.; Tang, W.-L. Variable-rate-supported adaptive synchronization in Ad-hoc network. *J. Xi'an Univ. Electron. Sci. Technol.* **2005**, *32*, 737–741.
24. Kislyy, S.A.; Pchenikin, I.A.; Kuzmin, I.A.; Khasanov, M.S.; Akashkin, E.L.; Lyalin, K.S. Research of the M-sequence Autocorrelation Function Side Lobe Suppression Due to the Cyclic Accumulation. In Proceedings of the 2022 IEEE International Multi-Conference on Engineering, Computer and Information Sciences (SIBIRCON), Yekaterinburg, Russian, 11–13 November 2022; pp. 2150–2154. [CrossRef]
25. Khanykov, I.; Nenashev, V.; Kharinov, M. Algebraic Multi-Layer Network: Key Concepts. *J. Imaging* **2023**, *9*, 146. [CrossRef]
26. Wang, X.; Yang, J.; Luo, Y. Multi-Channel Coupled Variational Bayesian Framework with Structured Sparse Priors for High-Resolution Imaging of Complex Maneuvering Targets. *Remote Sens.* **2025**, *17*, 2430. [CrossRef]
27. Nenashev, V.A.; Shepeta, D.A. Mathematical models and algorithms for modeling the location signals reflected from the underlying surfaces of the earth, sea, and coastal waters. In *Remote Sensing of the Ocean, Sea Ice, Coastal Waters, and Large Water Regions 2019*; SPIE: Bellingham, WA, USA, 2019; Volume 11150. [CrossRef]
28. Sun, H.; Yan, Y.; Liu, G.; Zhan, Y.; Li, X. CSOOC: Communication-State Driven Online–Offline Coordination Strategy for UAV Swarm Multi-Target Tracking. *Electronics* **2025**, *14*, 4743. [CrossRef]
29. Yaman, O. Development of a Closed-Loop PLM Application for Vibration-Based Structural Health Monitoring of UAVs. *Drones* **2025**, *9*, 807. [CrossRef]
30. Nenashev, V.A.; Khanykov, I.G.; Kharinov, M.V. A Model of Pixel and Superpixel Clustering for Object Detection. *J. Imaging* **2022**, *8*, 274. [CrossRef]
31. Sergeev, M.; Sentsov, A.; Nenashev, V.; Grigoriev, E. Triple-Station System of Detecting Small Airborne Objects in Dense Urban Environment. *Smart Innov. Syst. Technol.* **2021**, *238*, 83–93. [CrossRef]
32. Yi, J.; Fang, T.; Chai, L.; Wang, W.; Zheng, Y. Random Access Resource Configuration for LEO Satellite Communication Systems Based on TDD. *Telecom* **2025**, *6*, 94. [CrossRef]
33. Chen, D.; Zhang, Y.; Pang, G.; Gao, F.; Duan, L. A Hybrid Scheme for Disaster-Monitoring Applications in Wireless Sensor Networks. *Sensors* **2023**, *23*, 5068. [CrossRef]
34. Choi, J.-Y.; Jo, H.-S.; Mun, C.; Yook, J.-G. Preamble-Based Adaptive Channel Estimation for IEEE 802.11p. *Sensors* **2019**, *19*, 2971. [CrossRef]
35. Jeong, E.-R.; Lee, E.-S.; Joung, J.; Oh, H. Convolutional Neural Network (CNN)-Based Frame Synchronization Method. *Appl. Sci.* **2020**, *10*, 7267. [CrossRef]
36. Adam, M.S.; Por, L.Y.; Hussain, M.R.; Khan, N.; Ang, T.F.; Anisi, M.H.; Huang, Z.; Ali, I. An Adaptive Wake-Up-Interval to Enhance Receiver-Based Ps-Mac Protocol for Wireless Sensor Networks. *Sensors* **2019**, *19*, 3732. [CrossRef]
37. Wang, J.; Chen, H.; Duan, H.; Sun, R.; Yang, K.; Fang, J.; Xu, H.; Song, P. An Efficient RMA with Chunked Nonlinear Normalized Weights and SNR-Based Multichannel Fusion for MIMO-SAR Imaging. *Remote Sens.* **2025**, *17*, 3232. [CrossRef]
38. Cui, J.; Duan, J.; Guo, W.; Peng, C.; Li, H. SAR-ESAE: Echo Signal-Guided Adversarial Example Generation Method for Synthetic Aperture Radar Target Detection. *Remote Sens.* **2025**, *17*, 3080. [CrossRef]
39. Xin, J.; Liang, X.; Jiang, Z.; Li, H.; Dai, Y.; Wang, H.; Zhang, Y.; Bu, X. Robust Synchronization Error Estimation Under Multipath Fading in Distributed SAR. *Electronics* **2025**, *14*, 983. [CrossRef]

40. El-Awamry, A.; Zheng, F.; Kaiser, T.; Khaliel, M. Robust Peak Detection Techniques for Harmonic FMCW Radar Systems: Algorithmic Comparison and FPGA Feasibility Under Phase Noise. *Signals* **2025**, *6*, 36. [CrossRef]
41. Sun, D.; Li, A.; Ding, H.; Wei, J. Detection of DRFM Deception Jamming Based on Diagonal Integral Bispectrum. *Remote Sens.* **2025**, *17*, 1957. [CrossRef]
42. Yao, Z.; Fang, L.; Yang, J.; Zhong, L. Nonlinear Quantization Method of SAR Images with SNR Enhancement and Segmentation Strategy Guidance. *Remote Sens.* **2025**, *17*, 557. [CrossRef]
43. Guo, H.; Wang, F.; Li, N.; Wu, Z.; Pang, C.; Zhang, L.; Li, Y. A Detection and Cover Integrated Waveform Design Method with Good Correlation Characteristics and Doppler Tolerance. *Remote Sens.* **2025**, *17*, 1775. [CrossRef]
44. Wang, H.; Tao, H.; Zhong, T.; Li, W. Joint Transmit Waveform and Receive Mismatched Filter Design to Suppress Range Sidelobe. *Remote Sens.* **2025**, *17*, 175. [CrossRef]
45. Nenashev, V.A.; Bestugin, A.R.; Rabin, A.V.; Solenyi, S.V.; Nenashev, S.A. Modified Nested Barker Codes for Ultra-Wideband Signal-Code Constructions. *Sensors* **2023**, *23*, 9528. [CrossRef]
46. Nenashev, V.A.; Nenashev, S.A. Search and Study of Marked Code Structures for a Spatially Distributed System of Small-Sized Airborne Radars. *Sensors* **2023**, *23*, 6835. [CrossRef]